DOI: 10.24850/j-tyca-2022-01-01

Articles

Experimental-numerical study of the velocity field in a rectangular channel with composite curvature and variable width in 2DH

Estudio numérico-experimental del campo de velocidades en un canal rectangular con curvatura compuesta y ancho variable en 2DH

José Luis Aragón-Hernández[1], ORCID: https://orcid.org/0000-0001-5102-1598

Christian Alberto Caballero-Coranguez[2], ORCID: https://orcid.org/0000-0001-9080-7083

Amado Abel Jiménez-Castañeda[3], ORCID: https://orcid.org/0000-0003-2081-5429

Moisés Berezowsky-Verduzco[4], ORCID: https://orcid.org/0000-0002-7675-3450

[1]Department of Hydraulics, Division of Civil and Geomatic Engineering, Faculty of Engineering, Universidad Nacional Autónoma de México, Mexico City, Mexico, jaragonh@unam.mx

[2]Engineering Institute, Universidad Nacional Autónoma de México, Mexico City, Mexico, CCaballeroC@iingen.unam.mx

[3]Engineering Institute, Universidad Nacional Autónoma de México, Mexico City, Mexico, AJimenezC@iingen.unam.mx

[4]Engineering Institute, Universidad Nacional Autónoma de México, Mexico City, Mexico, mbv@pumas.ii.unam.mx

Corresponding author: José Luis Aragón-Hernández, jaragonh@unam.mx

Abstract

An analysis of the approximation obtained with the mathematical modeling systems HEC-RAS, Iber, and Telemac–Mascaret is presented, for calculating the velocity field in a rectangular section channel with compound curvature and variable width. On the channel, secondary currents and flow separation were developed; all three models are free to use and based on the horizontal two-dimensional flow (2DH) hypothesis. The Saint Venant equations are used in each mathematical model to calculate hydrodynamics and turbulence. The velocity field is determined from physical measurements in a laboratory channel with an acoustic Doppler velocimeter (Micro-ADV 16 MHz) and it is compared with the velocity fields calculated with the mathematical modeling systems (HEC-RAS, Iber, and Telemac-Mascaret). An error analysis is presented, with the aim of determining the degree of approximation obtained with each modeling system and of discussing the factors and phenomena observed

in the laboratory, this allows to have facts about the complexity and nature of turbulent flows in channels with strong bents. It was found that the three models, in general have similar and acceptable behavior, with an average approximation greater than 93 %; on the other hand, in an analysis by section, in a recirculation zone, flow separation and high turbulence were observed (physical processes of fluid dynamics that the models used cannot reproduce adequately), and so the average approximation decreases to 82.5 %.

Keywords: Bend channel, horizontal two-dimensional numerical modeling, hydrodynamics, turbulence, flow separation.

Resumen

Se presenta un análisis de la aproximación obtenida con los sistemas de modelación matemática HEC-RAS, Iber y Telemac–Mascaret para el cálculo del campo de velocidades en un canal de sección rectangular con curvatura compuesta y ancho variable; en el canal se desarrollaron corrientes secundarias y separación de flujo; los tres modelos son de uso libre y se basan en la hipótesis de flujo bidimensional horizontal (2DH). Se utilizan las ecuaciones de Saint Venant en cada modelo matemático para calcular la hidrodinámica y la turbulencia. El campo de velocidades se determina a partir de mediciones físicas en un canal de laboratorio con un velocímetro Doppler acústico (Micro-ADV 16 MHz) y se compara con los campos de velocidades calculados con los sistemas de modelación matemática (HEC-RAS, Iber y Telemac–Mascaret). Se presenta un

análisis de errores, con el objetivo de determinar el grado de aproximación obtenido con cada sistema de modelación, y la discusión de los factores y fenómenos observados en el laboratorio, esto permite tener conocimiento sobre la complejidad en la naturaleza de los flujos turbulentos en canales con curvaturas fuertes. Se encontró que los tres modelos, en general, tienen un comportamiento similar y aceptable, con una aproximación promedio superior al 93 %; en cambio, en un análisis por sección, en una zona de recirculación, se observó separación del flujo y alta turbulencia (procesos físicos de la dinámica del fluido que los modelos empleados no pueden reproducir de forma adecuada); la aproximación promedio disminuye hasta el 82.5 %.

Palabras clave: canal curvo, modelación numérica bidimensional horizontal, hidrodinámica, turbulencia, separación de flujo.

Received: 24/08/2020

Accepted: 02/12/2020

Introduction

A mathematical modeling system to calculate the velocity field in channels was presented by Jimenez and Berezowsky (2004), whose lateral boundaries have an irregular geometry or plane curves; they considered general curvilinear coordinates to adapt to these geometries and used the covariant version with physical components of the hydrodynamic equations, to approximate the solution to equations averaged in-depth, considering the hypothesis of horizontal two-dimensional flow; the differential equations were solved in finite differences with the MacCormack scheme (Garcia & Kahawita, 1986; Fennema & Chaudhry, 1990), which is of the explicit and second-order type; they included the calculation of turbulent viscosity (ν_t) with the parabolic and $k-\varepsilon$ models. In this work, five different geometries are presented in which the developed mathematical model is validated; experimental measurements and calculated velocity are presented, the process of calibration, verification, and validation of the numerical model is shown. The authors indicate that the comparison has a good approximation in almost all cases; however, in one of the applications, there are noticeable differences between the velocity fields measured and the calculated in a small area, mainly associated with limitations in the size of the calculation mesh, although they do not present an explanation that would allow to understand this variation between the measured and calculated velocity.

Luo (2013) presented a study of separation of flow and recirculation that occurs in channel expansions; he describes the calculation of velocity profiles, shear stress profiles (τ) due to turbulence, turbulent kinetic

energy profiles (k), as well as the energy dissipation rate and dispersion coefficient. The measured results were compared with those calculated by using a hydrodynamic model, which uses the equations averaged in-depth, and five turbulence models to calculate the turbulent viscosity (ν_t). A fundamental work to the analysis of hydrodynamics in bend channels was developed by Rozovskii (1957).

With the advancement of the state of knowledge in numerical methods, and the increase in the speed of computer equipment, nowadays, the Saint Venant equations in two dimensions are used for the calculation of hydrodynamics (Ghamry & Steffler, 2005; Luo, 2013), turbulence (Luo, 2013; Wu, Wang, & Chiba, 2004), secondary flows (Ghamry & Steffler, 2005; Song, Seo, & Kim, 2012), flow separation and recirculation (Luo, 2013) in curved channels, with acceptable results. For calculation of turbulence, the parabolic turbulence models, modified mix length, $k-\varepsilon$, $k-\varepsilon$ without equilibrium and RNG $k-\varepsilon$ are also included (Luo, 2013; Wu *et al*., 2004).

In previous works, discretization of the study domain can be analyzed with rectangular coordinates (Luo, 2013) and general curvilinear coordinates (Kalkwijk & De-Vriend, 1980; Jiménez & Berezowsky, 2004); In the first case, it entails limitations in the flexibility of the mesh and the calculation of solutions with discontinuities (Bladé *et al*., 2014b), whereas in the second case, it allows a better approximation in a representation of borders with curvature (Jiménez & Berezowsky, 2004).

Nowadays, there are different mathematical modeling systems, some contain their own fairly efficient mesh generators, with elements of

three (triangles), four (quadrilaterals), or more sides that allow a better approximation of the borders and refinement of the mesh in different areas. Among these models, those that are free to use stand out, mainly HEC-RAS, Iber, and Telemac-Mascaret; these models have been evaluated and compared with other models of academic (Horritt *et al*., 2007; Kaveh *et al*., 2019; Shustikova, Domeneghetti, Neal, Bates, & Castellarin, 2019) and commercial types (Pinos & Timbe, 2019; Rousseau, Biron, & Van-de-Wiel, 2016); all of them implemented in different hydraulic studies to calculate hydrodynamics in experimental devices and physical models (García & Matamoros, 2019; Hafnaoui & Debabeche, 2020), with good results.

The use of numerical models in engineering is an essential tool for designing hydraulic structures; their verification and validation allows to propose scenarios for decision-making, determine vulnerabilities, optimize hydraulic operation, among others. However, it is necessary to know the capabilities and limitations they offer, in order to avoid working with wrong solutions, therefore, it is essential to know the physics of the phenomenon and the criteria to choose optimal and efficient solutions (Bladé, Cea, & Corestein, 2014a). Thus, numerical models, as they are approximations, must be validated and verified, although this may be difficult to attain in direct applications in engineering, often because there are no data on measurements of variables in the field, such as levels of water, flows, velocities, temperature, or even more complex such as acceleration, transport of sediment from the bottom and suspension (Knight, 2014).

On the other hand, in experimental studies, the measurement of hydraulic variables with devices that have the adequate temporal and spatial resolution is very important (Voulgaris & Trowbridge, 1998). For this, sophisticated intrusive and non-intrusive measuring equipment with different technological advances are available. Recent research implements ultrasonic techniques with intrusive equipment to measure the velocity field, such as acoustic Doppler velocimeters (ADV), either point or vertical profilers (Voulgaris & Trowbridge, 1998; Lane *et al*., 1998); other recent non-intrusive visualization-based techniques such as particle tracking velocimetry (PIV, PTV), are gaining popularity (Ruonan, Liekai, Xingkui, & Danxun, 2016). A sample of the above is the velocity field measured with a Doppler-effect ultrasonic velocimetry profiler employed by Bombar, Elçi, Tayfur, Güney, and Bor (2011); similar works have been developed by Da-Silva, El-Tahawy, and Tape (2006); Abad and Garcia (2009); Termini (2009), and Abad, Frias, Buscaglia, and Garcia (2013), among others.

The objective of this work is to analyze the hydrodynamic behavior that develops in a channel with horizontal curves and variable width in the plan; this geometry was presented by Jiménez and Berezowsky (2004), essentially the velocity field from experimental measurements and the one determined by three mathematical models, HEC-RAS, Iber and Telemac-Mascaret. A comparison of the velocities and the analysis of errors in each of the models used are presented. This provides information about the behavior of hydrodynamics in curved channels, since in most cases, the geometries used are straight laboratory channels on which numerous applications have been validated, or that present a constant

width along a curve, as in the papers of Abad and Garcia (Abad & Garcia, 2006; Abad & Garcia, 2009), but the use of these numerical models in the application in river engineering shows more complex irregular geometries, which causes a turbulent flow, and makes the validation of the numerical models difficult with field measurements, and even establish the conditions at the borders for sceneries under study.

One of the advantages of these three models is that they are free to use and that all approximate a solution to the depth-averaged hydrodynamic equations, on structured and unstructured meshes, formed by elements of three (triangles), four (quadrilaterals), or more sides and include some models of turbulence.

This work consists of five sections: first, a description of the experimental set and its hydraulic operation, the measurement equipment used, and the tests carried out. Second, a brief description of the modeling systems used, as well as some of their main characteristics. Third, the results and a graphic comparison between the measured components of the velocity ($\overline{u}$ and $\overline{v}$) and those calculated numerically (bar indicates averages over time). Fourth, contains an analysis of the results and the differences in the comparison. Finally, the fifth includes the conclusions and recommendations for future works.

Materials and methods

Experimental set

The experimental set is a rectangular section channel with compound curvature (concave–convex-concave mixed curve with the radio of curvature of 1.67 m, 0.725 m, and 0.964 m, respectively), horizontal slope, variable width, and a horizontal length of 6.53 m (Figure 1).

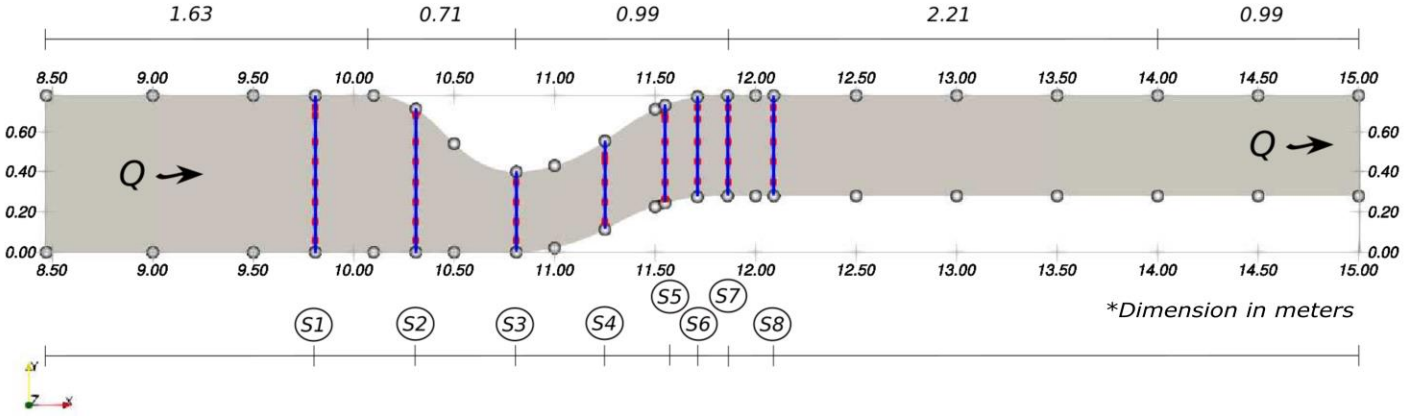

Figure 1. Geometry and dimensions of channel.

The channel begins with a straight section of 1.63 m in length and constant width horizontal bed ($b = 0.78\ m$). In plan, on the left bank (LB) width reduction begins due to the presence of the concave curve, which reaches a minimum width ($b = 0.40\ m$); up to this point right bank (RB) remains straight. After a convex curve appears on both margins, the channel immediately returns to a concave curvature until it reaches the initial straight path downstream, with both margins parallel.

The width of the section after the maximum contraction ($b = 0.40\ m$), has a gradual enlargement from 0.40 m to 0.50 m on the LB. The straight length of the channel outlet is 3.20 m. The bottom channel is steel and the side walls are glass. The section of the channel under study ranges from $X = 9.50\ m$ to $X = 13.0\ m$, with a ground area of 1,932 m^2 and a perimeter of 8,539 m. Eight cross-sections were fixed in which the punctual velocity measurements were made, located perpendicular to the X axis (Figure 1 and Table 1).

Table 1. Measurement, location, and width sections.

Section $[ID]$	$\boldsymbol{X}$ $[m]$	**width** $[m]$
S1	9.81	0.780
S2	10.31	0.713

S3	10.81	0.400
S4	11.25	0.441
S5	11.55	0.467
S6	11.71	0.478
S7	11.86	0.499
S8	12.09	0.500

When the width of the channel is less than 0.749 m, it could be considered narrow ($B/h < 5$) and with wall effects, but due to the material of the walls (glass) and bottom (steel), it is a channel with a hydraulically smooth wall and similar roughness, so it is not necessary to perform an analysis of this effect on the resistance to flow produced by wall friction in the velocity field, since it is considered negligible (Guo, 2017).

The point measurements of the three components of the velocity were obtained with an acoustic Doppler velocimeter (Micro-ADV 16 MHz), oriented in the vertical direction (with sensors pointing down). The detailed description of the operation of the measuring equipment is found in Kraus, Lohrmann, and Cabrera (1994); Lohrmann, Cabrera, and Kraus (1994); Anderson and Lohrmann (1995); Lane *et al.* (1998); Voulgaris and Trowbridge (1998); Nikora and Goring (1998); McLelland and Nicholas (2000), and López y Garcia (2001), among others. ADV was

placed on steel support that allows the instrument to be moved both horizontally and vertically, to control the position of the sensors within the flow and determine their relative position concerning one bank of the channel. The data collected over a period of time and with a certain frequency were analyzed with WinADV software (Wahl, 2000), first to determine the quality parameters and later the flow characteristics.

The quality of the collected data is defined by two parameters: the signal-to-noise ratio (SNR) and the correlation coefficient (COR) for each ADV receiver; the manufacturer recommends SNR values greater than 15 dB and a correlation coefficient greater than 70 %, to have an adequate description of the flow and turbulence characteristics; these parameters depend on particles and microbubbles that travel with the fluid or on the addition of seed particles (SonTek, 1997). In the experiments, data were filtered with SNR greater than 20 dB and 90 % correlation, so in this particular study, it was not necessary to introduce any type of seed particles to improve the measurements due to the turbulent nature of the flow.

Experimental test

The measurement campaign for test A (Table 2), consists of establishing an inlet flow of $Q = 10.3\, l/s$ supplied by a constant head tank, supplied by 2 pumping equipment of 5.0 hp each and measured with a thin-walled triangular spout with an angle of $90°$ located at $X = 0.00\, m$ (outlet flow reaches an underground gully generating a closed circuit); and a depth of $y = 0.149\, m$ m located at $X = 13.00\, m$ established by a flat vertical gate located at $X = 15.00\, m$; the previous conditions allowed establishing a subcritical and permanent flow in the channel.

Table 2. Experimental condition.

Test	$\boldsymbol{Q}$ $[l/s]$	$\boldsymbol{y}$ $[m]$	U_{s1} $[m/s]$	$\boldsymbol{S_w}$ $[x10^{-4}]$	$F_{r_{s1}}$ $-$	$R_{e_{s1}}$ $[x10^4]$	$\boldsymbol{h_m}$ $[m]$
A	10.3	0.149	0.088	4.3	0.072	1.32	0.06

The sampling volume to determine the velocity components were located at 40 % elevation of the depth, that is, $h_m = 0.4y$, measured from the channel bottom, that is, at 0.06 m (Table 2). The measurement of the velocity components was carried out at 45 points (Table 3), with a sampling frequency of 50 Hz for 180 s. With the information obtained from the 8 measurement points of section S1, the hydraulic variables indicated in Table 2 were determined.

Table 3. Measuring points

Point	Section	X $[m]$	Y $[m]$	Point	Section	X $[m]$	Y $[m]$
1	S1	9.81	0.720	24	S4	11.25	0.038
2	S1	9.81	0.680	25	S5	11.55	0.436
3	S1	9.81	0.550	26	S5	11.55	0.416
4	S1	9.81	0.450	27	S5	11.55	0.306
5	S1	9.81	0.350	28	S5	11.55	0.206
6	S1	9.81	0.250	29	S5	11.55	0.106
7	S1	9.81	0.150	30	S5	11.55	0.021
8	S1	9.81	0.060	31	S6	11.71	0.446
9	S2	10.31	0.680	32	S6	11.71	0.386
10	S2	10.31	0.550	33	S6	11.71	0.276
11	S2	10.31	0.450	34	S6	11.71	0.176
12	S2	10.31	0.350	35	S6	11.71	0.076

13	S2	10.31	0.250	36	S7	11.86	0.440
14	S2	10.31	0.150	37	S7	11.86	0.380
15	S2	10.31	0.060	38	S7	11.86	0.270
16	S3	10.81	0.350	39	S7	11.86	0.170
17	S3	10.81	0.250	40	S7	11.86	0.070
18	S3	10.81	0.150	41	S8	12.09	0.440
19	S3	10.81	0.060	42	S8	12.09	0.370
20	S4	11.25	0.368	43	S8	12.09	0.280
21	S4	11.25	0.338	44	S8	12.09	0.170
22	S4	11.25	0.238	45	S8	12.09	0.070
23	S4	11.25	0.138				

In Table 2, Q is the inlet flow, y is a depth located at $X = 13.00\ m$, U_{S1} is the mean velocity measured in section S1 (velocity of reference for the calculations presented ahead), which was obtained as the arithmetic average of the magnitude of the velocity of each of the 8 measurement points of section S1, S_w is the slope of the free surface of the water between sections S1-S8, h_m is the elevation of measurement from the

bottom, $F_{r_{s1}}$ and $R_{e_{s1}}$ are the Froude and Reynolds numbers in section S1, respectively.

From velocity measurements and water depth, it is determined that the free surface of the water tends to be horizontal, as indicated in Table 2. It was also observed that on the left bank of the channel, near section S4, an appreciable trail of small eddies forms on the free surface of the water.

Mathematical models

A brief description of the mathematical models used for the calculation of 2DH hydrodynamics is presented, as well as the references where more depth on the subject can be found.

HEC-RAS

HEC-RAS (Hydrologic Engineering Center-River Analysis System) mathematical modeling system is developed by the Hydrologic Engineering Center of the Institute of Water Resources, of the United States Corps of Engineers (US Army Corps of Engineers). This system allows the calculation of hydrodynamics in free-surface flows with the permanent and variable regime, in one and two dimensions, sediment transport and analysis of water quality, in networks of channels and rivers (HEC-RAS, 2016c).

The two-dimensional variable flow calculation module solves the diffusive wave equations or the Saint Venant equations, with the option of using the parabolic turbulence model. The equations are approximated with the methods of finite differences and finite volumes of the implicit type, which allows calculation time steps greater than those of the explicit type, and a robust wet-dry algorithm; calculation meshes can be structured and unstructured with up to 8 sides (HEC-RAS, 2016a; HEC-RAS, 2016b). In this work, the module corresponding to the calculation of horizontal two-dimensional flow with the Saint Venant equations and the parabolic turbulence model was used.

The study area is defined using RAS Mapper, the calculation mesh is elaborated (type, size, and several elements); subsequently, the hydraulic, initial, and boundary conditions are imposed; finally, the calculation data is defined.

Iber

Iber is a two-dimensional mathematical model for simulation of free surface flow, morphodynamics, transport processes, and habitat in rivers and estuaries, developed from the collaboration of the Water and Environment Engineering Group, GEAMA (Universidade da Coruña), the Group of Mathematical Engineering (Universidade de Santiago de Compostela), Flumen Institute (Universitat Politècnica de Catalunya y Centre Internacional de Mètodes Numèrics a l'Enginyeria) and promoted by the Center for Hydrographic Studies of CEDEX (Bladé *et al*., 2014b). It consists of different coupled modules, among them, the hydrodynamic and turbulence modules, which are used in this work.

The hydrodynamics module solves two-dimensional depth-averaged shallow water equations (SWE) to calculate the water depth and the two horizontal components of velocity (Bladé *et al*., 2014b); the turbulence modulus includes several models, one is the Boussinesq type, another is the depth averaging to calculate turbulent shear stresses (Cea, Puertas, & Vázquez-Cendón, 2007), and also the $k-\varepsilon$ model (Rastogi & Rodi, 1978). These equations are solved with a finite volume method of an explicit type in time, on structured and unstructured meshes with 3 and 4-sided elements (Bladé *et al*., 2014b). The pre-processing of the data

and post-processing of the results is carried out using the GiD tool (CIMNE, 2009).

In data preprocessing, the geometry of the study area is elaborated through the GiD interface, the hydraulic conditions, and the initial and boundary conditions are imposed; subsequently, the type, size, and a number of elements (calculation mesh) are defined and finally, the calculation data is defined.

Telemac-Mascaret

The Telemac-Mascaret 2D system makes it possible to approximate a solution to the free surface flow equations averaged in-depth (Hervouet, 2007). It is essentially based on the finite element technique and allows determining hydraulic quantities that are dependent on geometry. The calculation domain is discretized with triangular elements, and the calculation is developed in each node of the mesh, it also allows incorporating the effects of turbulence through the $k-\varepsilon$ model (Rastogi & Rodi, 1978) has additional modules such as water quality, sediment transport, among others (EDF-R&D, 2016).

In pre-processing, the geometry of the model (curved channel) is built and the boundary conditions are established, for this the Blue Kenue tool (CHC, 2011) is used to carry out the pre-processing and post-processing. The flow and turbulence equations are solved in a modular way using the fractional step method: first the advection is calculated using the characteristics method, then the propagation and diffusion (including turbulence) and the source terms in the dynamic equations, although there are recommendations to implement numerical schemes (Hervouet, 2007).

In the three models, the 2DH equations consider the hypothesis of hydrostatic pressure distribution and uniform velocity in the depth of the water, these hypotheses are well accepted in their application in river engineering.

Results

Discretization of the bent channel with HEC-RAS was carried out with 23,559 elements of 4 and 5 sides with average length and area of 0.009 m and 0.818 cm^2, respectively; in Iber with 1,277,640 4-sided elements

with a length of 0.001-0.0015 m and an average area of 0.015 cm^2, respectively; and with Telemac-Mascaret with 153,149 3-sided elements with a length of 0.001-0.005 m and an average area of 0.0126 cm^2, respectively. The type of mesh used in each model is indicated in Table 4.

Table 4. Calculation data.

Model	**Type of mesh**	**No. of elements**	**Turbulence model**	**CFL**	**Δt (s)**
HEC-RAS	Estructurada	23,559	Parabólico	-	0.10
Iber	Estructurada	1’277,640	k-ε	0.45	0.00016-0.0019
Telemac-Mascaret	No estructurada	153,149	k-ε	0.10	0.0015

In the three models, a depth of 0.149 m was used as an initial condition, in the inlet contour condition a flow of 0.0105 m^3/s and an outlet depth of 0.149 m. Bottom and wall friction was considered through a single Manning coefficient of friction of 0.011 $s/m^{1/3}$; this parameter was used to calibrate the models, that is, different values of the Manning coefficient of friction were proposed until the minimum differences

between the calculated and measured speed values were obtained. Regarding the increase in calculation time in HEC-RAS, the minimum allowed of 0.10 s was used, in Iber and Telema-Mascaret, those determined by the Courant-Friedrichs-Levy condition (CFL), which corresponds to 0.0016 s-0.00019 s and 0.0015 s, respectively. The turbulence model used in each model is shown in Table 4.

With the previous conditions, the calculation was carried out until permanent flow conditions were reached, this was achieved in a period of time of 6 minutes; in this way, the calculation times were 10 minutes with HEC-RAS, on a computer with an Intel Core i7-4770 processor, 3.4 GHz, 16 GB of RAM; 35.38 hours with Iber on a GeForce GTX 650 Ti graphics card from a computer with an Intel Core i7-4770 processor, 3.4 GHz, 16 GB of RAM; in the Telemac system, the optimization of the distributed computing process was developed in a cluster with 24 AMD processing cores, CentOS distribution, version 6.9, 64-bit architecture; for the parallel calculation, the message sending interface (MPI) was used, which allows the exchange of messages between the processors (Gropp, Lusk, & Skijellum, 2014) and METIS, which performs the distribution of the mesh between the number of processors, allowing the number of elements of the mesh to be the same for each processor, and thus minimize the number of adjacent elements, in order to balance the calculation between the processors (Karypis, 2013), so the calculation time was 3.67 hours.

Figure 2 shows the comparison of the calculated results with the measured data. In each illustration, the abscissa axis corresponds to the

velocity components $\overline{u}$ (left) and $\overline{v}$ (right) dimensionless with the mean velocity of section S1 (reference velocity); the axis of the ordinate corresponds to the location in the plan of the measurement point dimensionless with the total width of the cross-section of the channel.

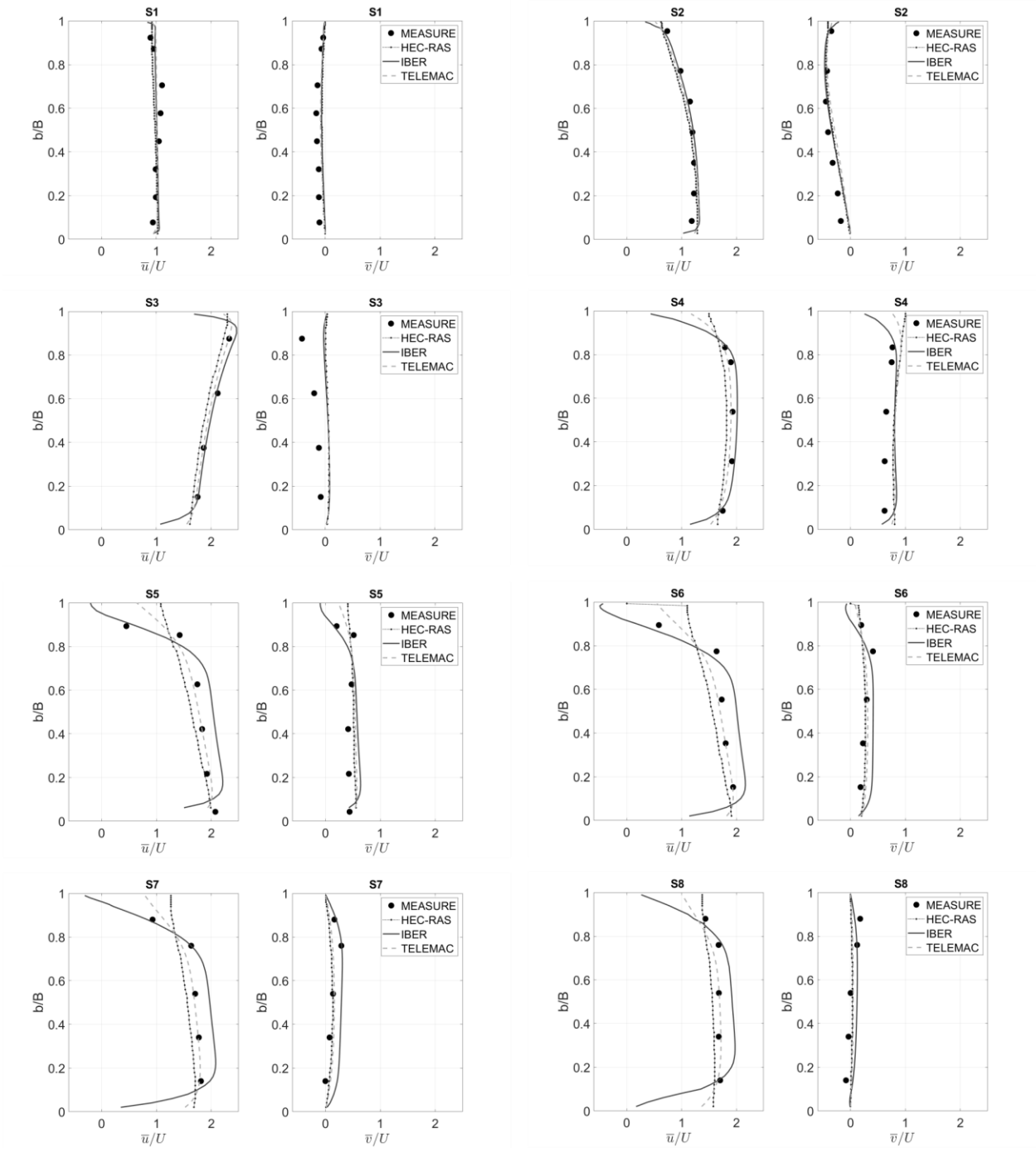

Figure 2. Numerical-experimental comparison of the horizontal components of velocity.

Additionally, to deepen the understanding of the hydrodynamics of the phenomenon that occurs between sections S3 and S7, the fields of the non-dimensional components of the velocity are presented with the mean velocity of section S1 (reference velocity) $\overline{u}/U_{S1}$ (Figure 3a) and $\overline{v}/U_{S1}$ (Figure 3b); the magnitude and gradient of the velocity (Figure 4), which shows the development of the cut layer; the kinetic energy of turbulence (Figure 5) and Reynolds number (Figure 6); all of them calculated by the Telemac-Mascaret model.

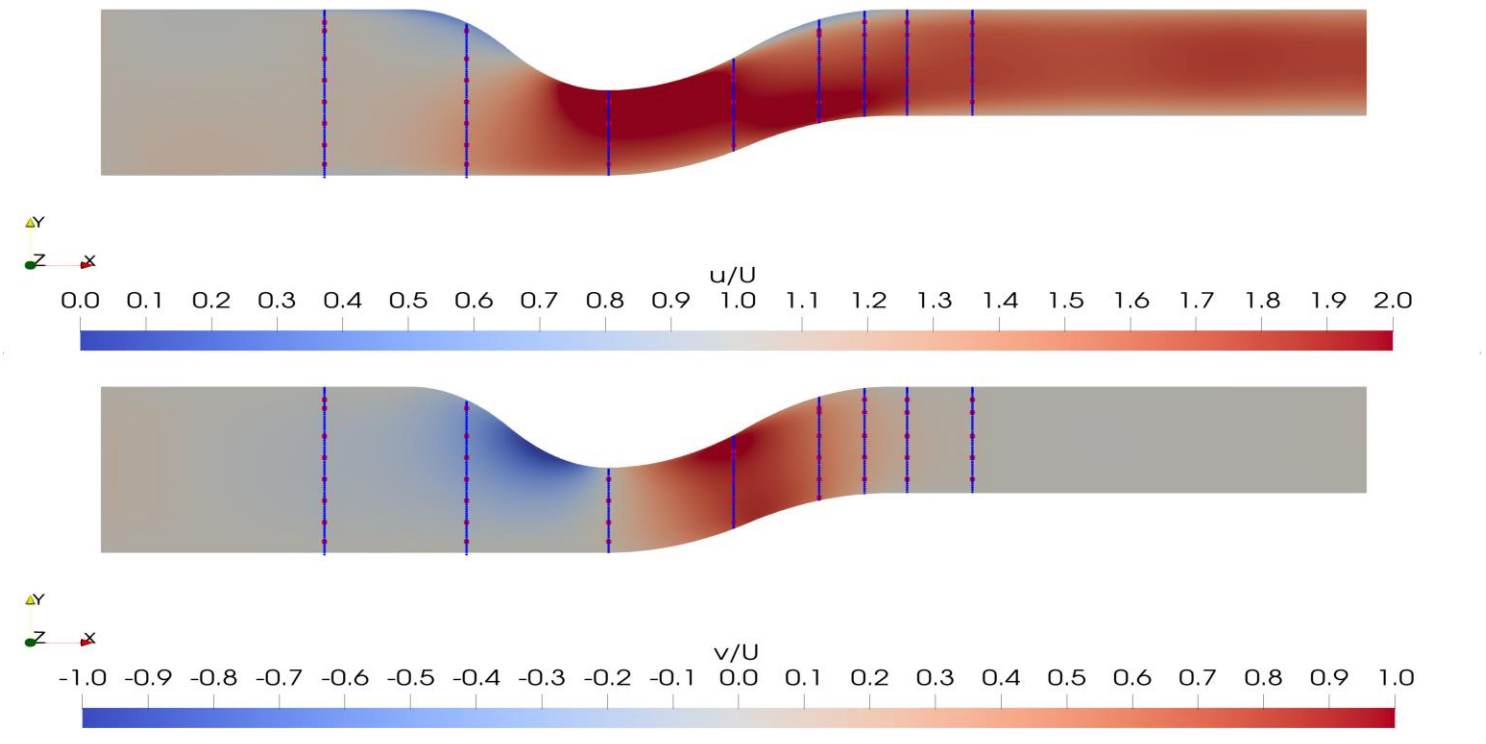

Figure 3. Velocity component fields.

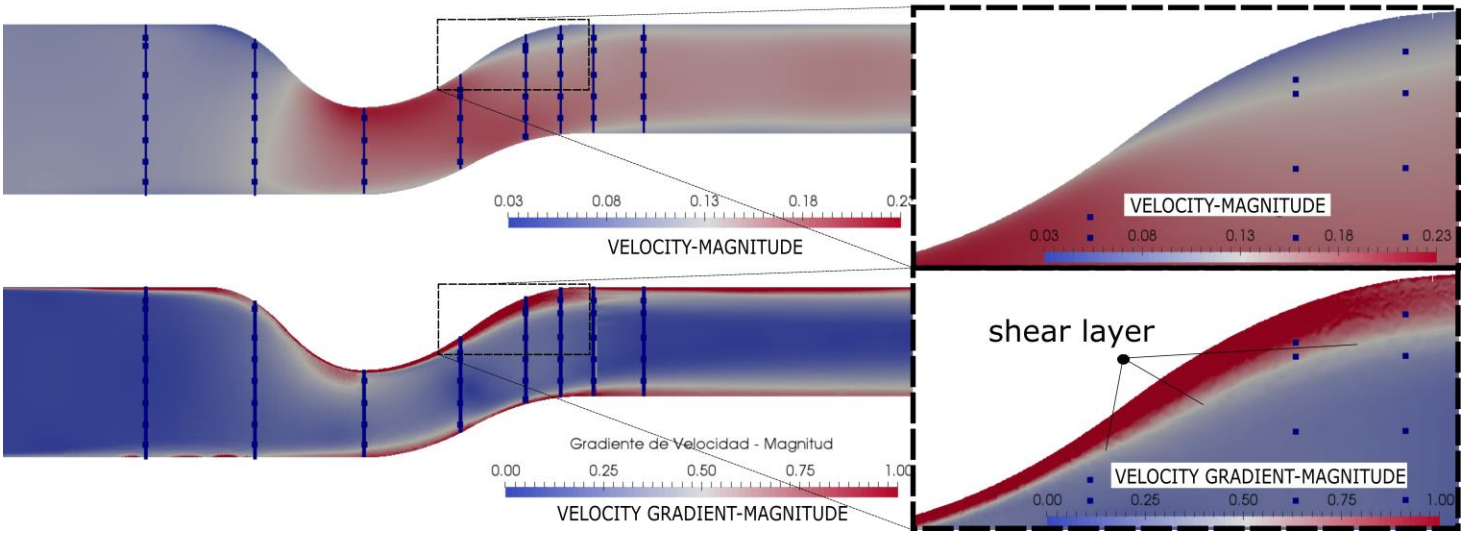

Figure 4. Velocity magnitude and gradient.

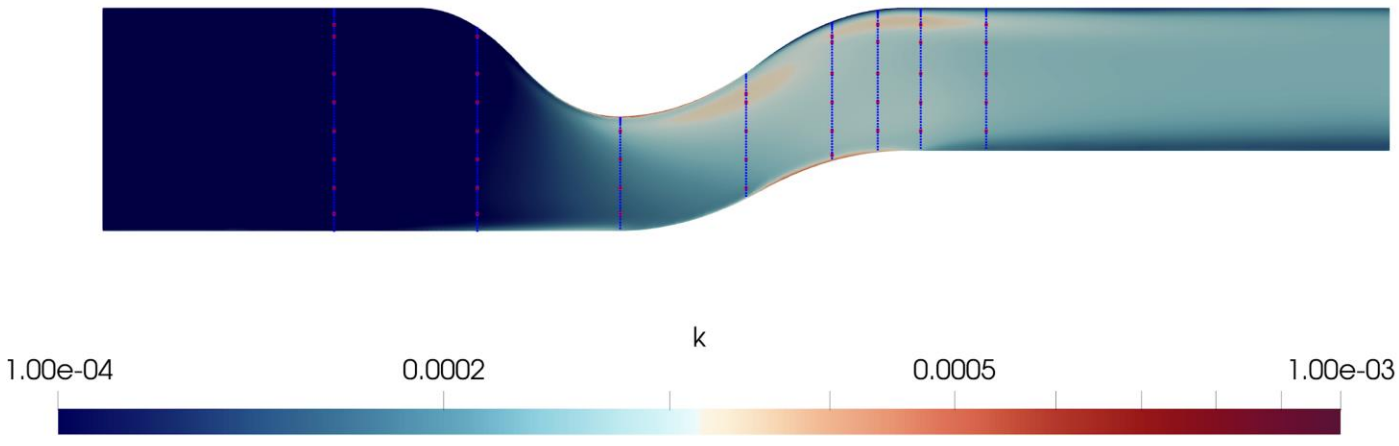

Figure 5. The kinetic energy of turbulence.

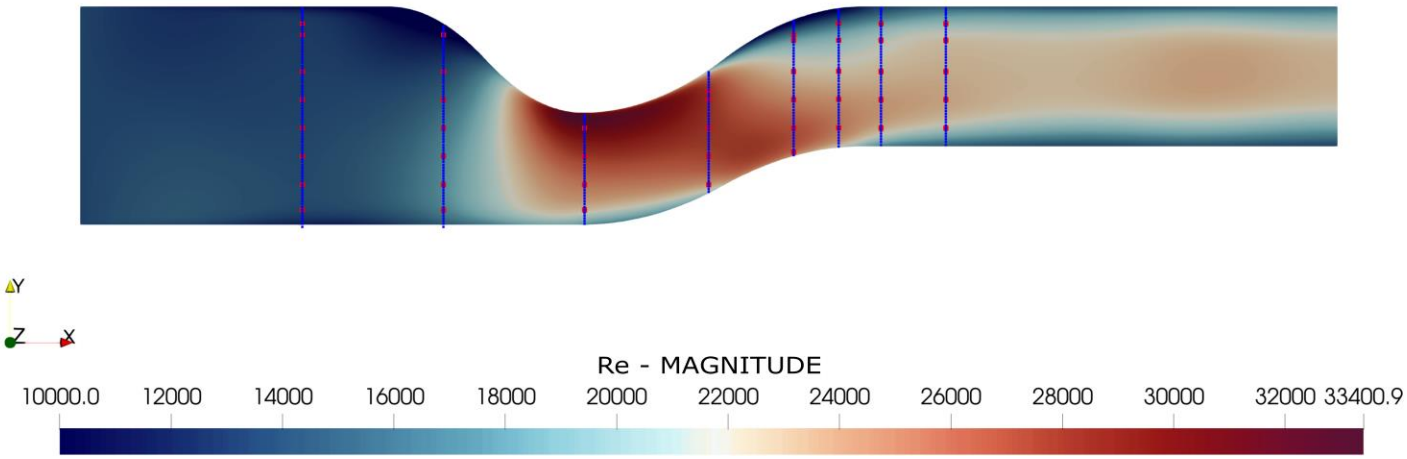

Table 6. Reynolds number.

Analysis and discussion of results

In general, the results calculated with the models used follow the trend of the measured values. Thus, in the first two sections (S1 and S2) the measured and calculated values are similar; on the other hand, in the following two sections (S3 and S4), this similarity is only maintained in the $\overline{u}$ component of the velocity, in the $\overline{v}$ component the three models have different behavior from the measured values. In the last four cross-

sections, even though the calculated values follow the trend of the measured values, there is a greater dispersion of these, but the results were slightly better than those reported by Jiménez and Berezowsky (2004). It was observed in all the cross-sections, that the results of the Telemac-Mascaret model are always between the results of HEC-RAS and Iber; With HEC-RAS, values lower than those measured on the right bank and higher on the left bank is obtained, on the other hand, with Iber the behavior of the values is the reverse, presumably, because it tries to adapt to the velocity profile near the walls; in these results, no improvement is perceived due to the increase in the number of elements, which is compatible with the results reported by Ghamry and Steffler (2005) in curved channels.

To know the performance of each model used, an error analysis was carried out between the measured and calculated values. Determining the difference of the numerical-experimental comparison is a complex task since there are always innate errors in the measurement process and those associated with the calibration of the models, the tools, and/or the measurement equipment. In addition to the above, there are the hydraulic and turbulent processes that intervene in the behavior of the flow, remember that currently, turbulence continues to be an unsolved phenomenon.

Additionally, the measurement of a variable reduces the uncertainty about its behavior as long as specific criteria are followed, in order to minimize the different types of errors; by having a record of their behavior over time and by processing this information, it is possible to consider

which part of the measurement record is acceptable and which is not, through quality parameters (SNR and COR).

Thus, in order to determine the approximation offered by each of the numerical models, a simple linear regression analysis is proposed to estimate the relationship between the measured velocity and the one calculated by the numerical models used. Starting from the point of view that different types of innate errors can occur in the measurement process, and that numerical models are approximations to the solution of equations, in this particular case 2DH or SWE, and that they are not an exact solution of the behavior of a free surface flow, and in addition to the hypothesis that the behavior variation of the velocity distribution in the vertical can be replaced by an average, the indicated relationship can be established.

Figure 7 presents this analysis for the 45 measurement points of the three velocity variables ($\overline{U}$, $\overline{u}$ and $\overline{v}$); the results are shown dimensionless as: $\overline{U}_m = \frac{|\overline{U}|_{measure}}{U_{S1}}$, $\overline{U}_{cal} = \frac{|\overline{U}|_{calculated}}{U_{S1}}$, $\overline{u}_{x_{med}} = \frac{\overline{u}_{x_{measure}}}{U_{S1}}$, $\overline{u}_{y_{med}} = \frac{\overline{u}_{y_{measure}}}{U_{S1}}$, $\overline{u}_{x_{cal}} = \frac{\overline{u}_{x_{calculated}}}{U_{S1}}$, $\overline{u}_{y_{cal}} = \frac{\overline{u}_{y_{calculated}}}{U_{S1}}$. The continuous line represents the expected relationship (RE) considered as optimal, which indicates that the measured speed must be equal to the calculated speed or vice versa; the points correspond to the relationship between measured and calculated speed (RMC); finally, the existing correlation is determined and shown by a simple linear regression with a dashed line (RL) and its corresponding correlation coefficient (R), which allows determining the

goodness of fit of the regression model (Menhenhall et al. 2010). Table 5 presents the correlation coefficients R.

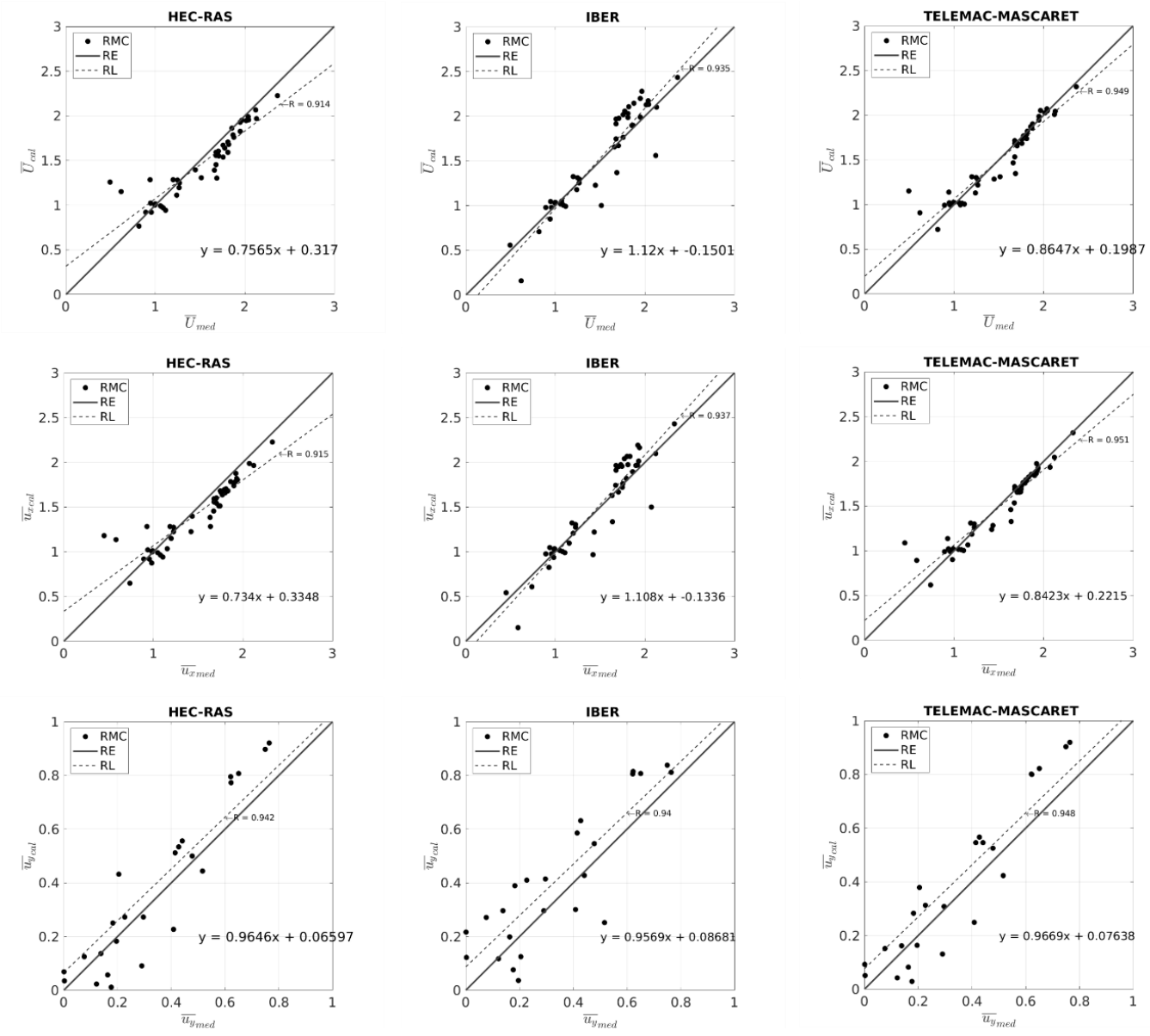

Figure 7. Linear regression models.

Table 5. Correlation coefficients for the 45 measurement points.

Model/Variable	$R_{\overline{U}}$	$R_{\overline{u}}$	$R_{\overline{v}}$
HEC-RAS	0.914	0.915	0.942
Iber	0.935	0.937	0.940
Telemac-Mascaret	0.949	0.951	0.948

From the analysis above, it is observed that the lowest correlation values correspond to HEC-RAS, while the highest to Telemac-Mascaret, Iber is very close to the average value, although for engineering purposes all three models are acceptable.

The procedure described was also performed for the measurement points of the three variables of the velocity of each section; the correlation coefficients are presented in Table 6. In particular, it is highlighted that with the three models in section S1 the lowest correlations are obtained, being very low for the magnitude of the speed and the components; when reviewing the settings in this section, it is observed that the models tend to underestimate for velocities greater than the unit and overestimate when the velocity is less than the unit, this has to do with the process of eliminating the average velocity, because small fluctuations remain that do not tend to fit a linear model with a 45° line, but rather a horizontal line with an ordinate at the origin very close to the unit, it is also the

section in which the reference speed is determined; the next section with the lowest correlation coefficient in the three models, corresponds to section S5. It is also observed that HEC-RAS results in low correlation coefficients in the velocity component $\overline{v}$.

Table 6. Correlation coefficients for the points of each measurement section.

Mod.	**HEC-RAS**			**Iber**			**Telemac-Mascaret**		
S/V	$\overline{U}$	$\overline{u}$	$\overline{v}$	$\overline{U}$	$\overline{u}$	$\overline{v}$	$\overline{U}$	$\overline{u}$	$\overline{v}$
S1	0.101	0.085	-0.896	0.023	0.023	0.002	0.378	0.378	0.292
S2	0.925	0.899	0.467	0.959	0.959	0.935	0.938	0.938	0.920
S3	0.995	0.995	0.985	0.992	0.992	0.992	0.995	0.995	0.995
S4	0.950	0.802	0.103	0.981	0.981	0.976	0.985	0.985	0.952
S5	0.822	0.820	0.660	0.819	0.819	0.818	0.890	0.890	0.889
S6	0.822	0.815	0.878	0.965	0.965	0.964	0.920	0.920	0.918
S7	0.832	0.829	0.581	0.979	0.979	0.978	0.942	0.942	0.941
S8	0.791	0.791	0.478	0.873	0.873	0.874	0.917	0.917	0.917

The numerical-experimental comparison is acceptable if the correlation coefficient tends to 1 or −1, and in section S5 it is less than 0.9; an intermittent recirculation zone was observed on the left margin of section S5 in laboratory tests; it was determined that it corresponds to a zone of separation of the flow and beginning of eddies that propagate downstream, so it could be a reason for the low correlation.

On the other hand, the plan shape of the channel (compound curvature and variable width), causes a particular behavior of the flow, typical of meandering rivers. Thus, the decrease in channel width from 0.78 m (S1) to 0.40 m (S3), due to the presence of the concave-convex curve, on the left margin of the channel, first generates a decrease in the velocity component $\overline{u}$ (Figure 3a) and then negative velocities in component $\overline{v}$ (Figure 3b), in the vicinity of section S2. In section S3, the flow accelerates and the velocity in component $\overline{u}$ increases; it holds up to section S7 (Figure 3a). The convex-concave curve that allows the expansion of the channel width from 0.40 m to 0.50 m, on the left margin (S3 to S7) there is a non-symmetric expansion that causes an increase in the velocity component $\overline{v}$ (Figure 3b) and a decrease in the velocity component $\overline{u}$ (Figure 3a), that is, a velocity gradient between sections S5 to S7 (Figure 4b); behavior that the models used cannot reproduce.

Delving in the same direction, the velocity gradient (Figure 4b) generates the development of a shear layer (velocities lower than those of the main flow), indicated by a thin curve in Figure 4b; the flow between the left wall and the cut layer is highly turbulent and presents low velocities, compared to the velocities of the main flow (Figure 4a), flow

separation (red color in Figure 4b); these hydraulic processes in this work are analyzed in 2D, but in essence, they are in 3D, so that the fluctuations of the speed (u' and v') increase and this is reflected in the kinetic energy of the turbulence (k) (Figure 6), mainly on the left margin between sections S5-S7, an area where the calculated velocity values differ from the measured values.

Finally, the behavior of the Reynolds number, which allows us to establish and understand the importance of the relationship of inertial forces (acceleration) and viscous forces (friction) (Çengel & Cimbala, 2010), shows the acceleration of the flow when considering that variations in viscous forces are small, this also indicates that the effects of wall roughness are negligible.

Conclusions and recommendations

In this work, the numerical-experimental comparison of the velocity components and their magnitude in a rectangular channel with compound horizontal curvature, and the values calculated with three free-use two-dimensional mathematical modeling systems most used in practice in

river engineering, was carried out for the calculation of hydrodynamics and turbulence.

From the error analysis performed on the 45 measured points, it is determined that the three models have similar and acceptable behavior, with an average approximation of the three variables of the speed greater than 93 %, with Telemac-Mascaret (94.9 %) being a slightly better approach, then Iber (93.7 %) and finally HEC-RAS (92.4 %). However, when evaluating the speed variables per section, the approximation in the $\overline{v}$ component with HEC-RAS decreases to 40.7 %, while Iber presents an approximation of 81.7 % and Telemac-Mascaret of 85.3 %.

By observing the fields of the velocity components, it is determined that $\overline{u}$ increases shortly before the section S3 does not appear uniformly across the width of the section and is mainly concentrated in the left margin, after the maximum velocity core passes from MI to MD (sections S3 to S5); for component $\overline{v}$, the maximum velocity is concentrated near the MI in section S5, and the minimum in the same range between sections S2 and S3.

The Reynolds number indicates a turbulent flow, if it's considered that the variation of the characteristic length is similar throughout the channel and the variation of the viscosity is small, it allows us to observe the acceleration of the flow. Thus, an area near the left bank is identified where the relationship is lower, that is, the flow decelerates on the left bank between sections S4 to S8. Also, the development of the cut layer is determined with the flow velocity gradient (Figure 4b). This layer affects the flow distribution after section S4, causing the main flow to deviate

towards the center and MD of the channel, concentrating the maximum velocity core in this margin. The area between the BL and the shear layer is a flow separation zone, the product of the gradual expansion in the width of the channel, which allows the development of secondary flows, since when the velocity $\overline{u}$ decreases, and although the Reynolds number decreases within this zone, the kinetic energy of turbulence (k) increases; Based on the above, one of the important conclusions is that this zone cannot be reproduced by numerical models based on the Saint Venant hypothesis, and this is demonstrated by the numerical-experimental comparison of the velocities shown in Figure 2, in the points located near the MI between sections S5-S8.

In general, the hydrodynamics of the channel with the presented geometry, calculated by the numerical models used, has on average an approximation greater than 93 %, following the hypothesis that the velocity field located at 0.6 of the depth of the flow, which for engineering application is acceptable. The area of least approximation (left margin of sections S4-S7) casts doubt on the 2DH hypothesis, since it is much more complex to reproduce, and the numerical model is not adequate. However, this phenomenon is important since expansion can considerably affect flow redistribution, mainly in hydraulic structures, which is where adequate flow control is needed, so the analysis presented must be considered in the design. The application itself of this analysis in meandering rivers also raises a line of research due to the effects on the migration of the banks when receiving the incidence of the flow in them, as well as the phenomenon of sediment transport, and the interaction of

the evolution of the bottom and the adaptation of the flow, which undoubtedly modifies its behavior.

Finally, it is recommended to expand the measurements with a greater number of points, measured at different depths, expand to the area that is not reproducible in this work, to improve the knowledge of the flow behavior in curved channels, this to delve into the lines of research proposed.

Acknowledgment

The authors are grateful for the support of the Dirección General de cómputo y Tecnologías de Información y Comunicación (DGTIC) de la Universidad Nacional Autónoma de México (UNAM), for the supercomputer resources for the development of the numerical calculations assigned under the LANDCAD-project UNAM-DGTIC-389, and Departamento de Sistemas Linux y Súper Cómputo de la Secretaría de Telecomunicaciones e Informática del Instituto de Ingeniería, UNAM.

References

Abad, J. D., Frias, C. E., Buscaglia, G. C., & Garcia, M. H. (2013). Modulation of the flow structure by progressive bedforms in the Kinoshita meandering channel. *Earth Surface Processes and Landforms*, 38(13), 1612-1622. DOI: 10.1002/esp.3460

Abad, J. D., & Garcia, M. H. (2006). Hydrodynamics in Kinoshita-generated meandering bends: Importance for river-planform evolution. *River, Coastal and Estuarine Morphodynamics: RCEM 2005-Proceedings of the 4th IAHR Symposium on River, Coastal and Estuarine Morphodynamics*, Urbana, USA, 2(1), 761-771.

Abad, J. D., & Garcia, M. H. (2009). Experiments in a high-amplitude Kinoshita meandering channel: 1. Implications of bend orientation on mean and turbulent flow structure. *Water Resources Research*, 45(2). DOI: 10.1029/2008WR007016.

Anderson, S., & Lohrmann, A. (1995). *Open water test of the SonTek acoustic Doppler velocimeter*. St. Petersburg, FL, USA: Proceedings of the IEEE Fifth Working Conference on Current Measurement, 188–192. DOI:10.1109/ccm.1995.516172

Bladé, E., Cea, L., & Corestein, G. (2014a). Modelización numérica de inundaciones fluviales. *Ingeniería del Agua*, 18(1), 71–82.

Bladé, E., Cea, L., Corestein, G., Escolano, E., Puertas, J., Vászquez-Cendón, M. E., Dolz, J., & Coll, A. (2014b). Iber: herramienta de simulación numérica del flujo en ríos. *Revista Internacional de Métodos Numéricos para cálculo y diseño en en Ingeniería*, 30(1), 1-10. DOI: 10.1016/j.rimni.2012.07.004

Bombar, G., Elçi, Ş., Tayfur, G., Güney, M. Ş., & Bor, A. (2011). Experimental and numerical investigation of bed-load transport under unsteady flows. *Journal of Hydraulic Engineering*, 137(10), 1276-1282. DOI: 10.1061/(asce)hy.1943-7900.0000412

Cea, L., Puertas, J., & Vázquez-Cendón, M. E. (2007). Depth averaged

modelling of turbulent shallow water flow with wet-dry fronts. *Archives of Computational Methods in Engineering*, 14(3), 303-341. DOI:10.1007/s11831-007-9009-3

Çengel, Y. A., & Cimbala, J. M. (2010). *Fluid mechanics. Fundamentals and applicactions*. New York, USA: McGrawHill.

CHC, Canadian Hydraulics Centre. (2011). *Blue Kenue Reference manual*. Ontario, Canada: Canadian Hydraulics Centre, National Research Council.

CIMNE, Centre Internacional en Mètodes Numèrics a l'Enginyeria. (2009). *GiD. The universal, adaptative and user friendly pre and postprocessing system for computer analysis in science and engineering. Reference manual*. Recovered from http://www.gidhome.com

Da-Silva, A. M. F., El-Tahawy, T., & Tape, W. D. (2006). Variation of flow pattern with sinuosity in sine-generated meandering streams. *Journal of Hydraulic Engineering*, 132(10), 1003-1014. DOI: 10.1061/(asce)0733-9429(2006)132:10(1003)

EDF-R&D. (2016). *Telemac modelling system. 3D hydrodynamics. Operating manual* (release 7.1). Francia: EDF-R&D.

Fennema, R. J., & Chaudhry, M. H. (1990). Explicit Methods for 2-D transient free surface flows. *Journal of Hydraulic Engineering*, 116(8), 1013-1034. DOI: 10.1061/(ASCE)0733-9429(1990)116:8(1013)

García, D. A., & Matamoros, H. (2019). Análisis y comparación de los resultados de la simulación de flujo de un modelo físico a escala con el modelo numérico utilizado por el software IBER 2D. *Revista de la Escuela Colombiana de Ingeniería*, 114(2019), 77-85.

Garcia, R., & Kahawita, R. A. (1986). Numerical solution of the St. Venant equations with MacCormack finite-difference Scheme. *International Journal for Numerical Methods in Fluids*, 6(5), 259-274. DOI: 10.1002/fld.1650060502

Ghamry, H. K., & Steffler, P. M. (2005). Two-dimensional depth-averaged modeling of flow in curved open channels. *Journal of Hydraulic Research*, 43(1), 44-55. DOI: 10.1080/00221680509500110

Gropp, W., Lusk, E., & Skijellum, A. (2014). *Using MPI: Portable parallel programming with the message-passing interface* (3rd ed.). Cambridge, USA: The MIT Press.

Guo, J. (2017). Exact procedure for Einstein-Johnson's sidewall correction in open channel flow. *Journal Hydraulic Engineering*, 143(4), 06016027. DOI: 10.1061/(asce)hy.1943-7900.0001260

Hafnaoui, M. A., & Debabeche, M. (2020). Numerical modeling of the hydraulic jump location using 2D Iber software. *Modeling Earth Systems and Environment*. DOI: 10.1007/s40808-020-00942-3

HEC-RAS. (2016a). *2D Modelling user's manual. River Analysis System* (version 5.0). Davis, USA: Hydrologic Engineering Center, Institute for Water Resources, U. S. Army Corps of Engineers.

HEC-RAS. (2016b). *Hydraulic reference manual. River Analysis System* (version 5.0). Davis, USA: Hydrologic Engineering Center, Institute for Water Resources, U. S. Army Corps of Engineers.

HEC-RAS. (2016c). *User's manual. River Analysis System* (version 5.0). Davis, USA: Hydrologic Engineering Center, Institute for Water Resources, U. S. Army Corps of Engineers.

Hervouet, J. M. (2007). *Hydrodynamics of free surface flows: Modelling with the finite element method*. Chichester, England: John Wiley and Sons, Ltd. DOI: 10.1002/9780470319628

Horritt, M. S., Di-Baldassarre, G., Bates, P. D., & Brath, A. (2007). Comparing the performance of a 2-D finite element and a 2-D finite volume model of floodplain inundation using airborne SAR imagery. *Hydrological Processes*, 21(20), 2745-2759. DOI: 10.1002/hyp.6486

Jiménez, A. A., & Berezowsky, M. (2004). *Modelación del flujo bidimensional horizontal con coordenadas curvilíneas generales* (SID 641). Ciudad de México, México: Instituto de Ingeniería, Universidad Nacional Autónoma de México.

Kalkwijk, J. P. T., & De-Vriend, H. J. (1980). Computation of the flow in shallow river bends. *Journal of Hydraulic Research*, 18(4), 327-342. DOI: 10.1080/00221688009499539

Karypis, G. (2013). *METIS. A software package for partitioning unstructured graphs and computing fill-reduced orderings of sparse matrices* (version 5.1.0.). Minneapolis, USA: Department of Computer Science & Engineering, Univesity of Minnesota.

Kaveh, K., Reisenbüchler, M., Lamichhane, S., Liepert, T., Nguyen, N. D., Bui, M. D., & Rutschmann, P. (2019). A comparative study of comprehensive modeling systems for sediment transport in a curved open channel. *Water* (Switzerland), 11(9). DOI: 10.3390/w11091779

Knight, D. W. (2014). River hydraulics - A view from midstream. *Journal of Hydraulic Research*, 52(1), 138-139. DOI: 10.1080/00221686.2013.855270

Kraus, N. C., Lohrmann, A., & Cabrera, R. (1994). New acoustic meter for measuring 3D laboratory flows. *Journal of Hydraulic Engineering*, 120(3), 406-412. DOI: 10.1061/(ASCE)0733-9429(1994)120:3(406)

Lane, S. N., Biron, P. M., Bradbrook, K. F., Butler, J. B., Chandler, J. H., Crowell, M. D., McLelland, S. J., Richards, K. S., & Roy, A. G. (1998). Three-dimensional measurement of river channel flow processes using acoustic Doppler velocimetry. *Earth Surface Processes and Landforms*, 23(13), 1247-1267. DOI: 10.1002/(SICI)1096-9837(199812)23:13<1247::AID-ESP930>3.0.CO;2-D

Lohrmann, A., Cabrera, R., & Kraus, N. C. (1994). Acoustic-Doppler velocimeter (ADV) for laboratory use. *Proceedings of the Symposium on Fundamentals and Advancements in Hydraulic Measurements and Experimentation* (pp. 351-365), ASCE, Buffalo, USA.

López, F., & Garcia, M. H. (2001). Mean flow and turbulence structure of open-channel flow through non-emergent vegetation. *Journal of Hydraulic Engineering*, 127(5), 392-402. DOI: 10.1061/(ASCE)0733-9429(2001)127:5(392)

Luo, E. C. R. (2013). Hydrodynamic characteristics of expanded channels with their applications -the state-of-the-art. *American Journal of Civil Engineering*, 1(1), 31-40. DOI: 10.11648/j.ajce.20130101.15

McLelland, S. J., & Nicholas, A. P. (2000). A new method for evaluating errors in high-frequency ADV measurements. *Hydrological Processes*, 14(2), 351-366. DOI: 10.1002/(sici)1099-1085(20000215)14:2<351::aid-hyp963>3.3.co;2-b

Menhenhall, W., Beaver, R. J., & Beaver, B. M. (2010). *Introducción a la*

probabilidad y estadística (13ª ed.). México, DF, México: Cengage Learning.

Nikora, V., & Goring, D. (1998). ADV measurements of turbulence: Can we improve their interpretation? *Journal of Hydraulic Engineering*, 124(6), 630-634. DOI: 10.1061/(ASCE)0733-9429(1998)124:6(630)

Pinos, J., & Timbe, L. (2019). Performance assessment of two-dimensional hydraulic models for generation of flood inundation maps in mountain river basins. *Water Science and Engineering*, 12(1), 11-18. DOI: 10.1016/j.wse.2019.03.001

Rastogi, A. K., & Rodi, W. (1978). Predictions of heat and mass transfer in open channels. *Journal Hydraulics Division*, 104(3), 397-420.

Rousseau, Y. Y., Biron, P. M., & Van-de-Wiel, M. J. (2016). Sensitivity of simulated flow fields and bathymetries in meandering channels to the choice of a morphodynamic model. *Earth Surface Processes and Landforms*, 41(9), 1169-1184. DOI: 10.1002/esp.3885

Rozovskii, I. L. (1957). *Flow of water in bends of open channels*. Kiev, Ukraine: Academy of Sciences of the Ukrainian SSR.

Ruonan, B., Liekai, C., Xingkui, W., & Danxun, L. (2016). Comparison of ADV and PIV measurements in open channel flows. *Procedia Engineering* (12th International Conference on Hydroinformatics (HIC 2016)-Smart Water for the Future), 154, 995-1001. DOI: 10.1016/j.proeng.2016.07.588

Shustikova, I., Domeneghetti, A., Neal, J. C., Bates, P., & Castellarin, A. (2019). Comparing 2D capabilities of HEC-RAS and LISFLOOD-FP on complex topography. *Hydrological Sciences Journal*, 64(14), 1769-

1782. DOI: 10.1080/02626667.2019.1671982

Song, C. G., Seo, I. W., & Kim, Y. D. (2012). Analysis of secondary current effect in the modeling of shallow flow in open channels. *Advances in Water Resources*, 41(2012), 29-48. DOI: 10.1016/j.advwatres.2012.02.003

SonTek. (1997). *Pulse coherent Doppler processing and the ADV correlation* (November). San Diego, USA: SonTek Technical Note.

Termini, D. (2009). Experimental observations of flow and bed processes in large-amplitude meandering flume. *Journal of Hydraulic Engineering*, 135(7), 575-587. DOI: 10.1061/(asce)hy.1943-7900.0000046

Voulgaris, G., & Trowbridge, J. H. (1998). Evaluation of the acoustic doppler velocimeter (ADV) for turbulence measurements. *Journal of Atmospheric and Oceanic Technology*, 15(1), 272-289. DOI: 10.1175/1520-0426(1998)015<0272:eotadv>2.0.co;2

Wahl, T. L. (2000). Analyzing ADV data using WinADV. *Joint Conference on Water Resource Engineering and Water Resources Planning and Management*, Minneapolis, USA. DOI: 10.1061/40517(2000)300

Wu, W., Wang, P., & Chiba, N. (2004). Comparison of five depth-averaged 2-D turbulence models for river flows. *Archives of Hydro-Engineering and Environmental Mechanics*, 51(2), 183-200.